applied sciences

MDPI

Article

Experimental Study on Improving the Impermeability of Concrete under High-Pressure Water Environments Using a Polymer Coating

Baobao Tan [1], Long Qu [2], Yong Xia [3], Xingyi Yang [3], Bo Su [1], Jiaqi Wu [2] and Mingli Xiao [2,*]

[1] Guoneng Sichuan Ashui Power Development Corporation Limited, Maerkang 624000, China
[2] State Key Laboratory of Hydraulics and Mountain River Engineering, College of Water Resource and Hydropower, Sichuan University, Chengdu 610065, China
[3] POWERCHINA Chengdu Engineering Corporation Limited, Chengdu 610072, China; yangxingyi1980@163.com (X.Y.)
* Correspondence: xiaomingli@scu.edu.cn; Tel.: +86-138-8065-3644

Abstract: The concrete lining of high-pressure water conveyance tunnels permeates under high-pressure water. Dense and hydrophobic coating can effectively improve the impermeability of concrete. However, the coating exhibits varying impermeability in different high-pressure environments, which can even lead to coating detachment or damage. The objectives of this study are to improve the high-pressure impermeability of concrete by using a polymer coating, and to study the varying impermeability through experiments. This study applied a polymer coating called SCU-SD-SP-II (SSS) to concrete surfaces, and it formed a composite protective layer with an epoxy-modified silicone (EMS) coating. A series of high-pressure impermeability tests were conducted to study the seepage regulation of the coated concrete and the failure mechanism of the SSS coating under cracks in the concrete. The results indicate that the SSS coating has excellent impermeability. Pressurized water of 3 MPa could not permeate the SSS coating with a thickness of 0.5 mm within 24 h. Under both external and internal water pressure conditions, the SSS coatings improved concrete impermeability. Additionally, the average seepage height and relative permeability coefficient of the latter decreased by 49.6% and 71.2%, respectively, compared with the former. After concrete cracking, the SSS coating could withstand 3 MPa pressure on crack surfaces smaller than 1 mm. When the crack width was greater than 2 mm, the SSS coating deformed under 1 MPa pressure. As the pressure increased to 2 MPa or even 3 MPa, the SSS coating was punctured or torn due to stress concentration. This study provides new insights into the impermeability of concrete under high water pressure.

Keywords: high water pressure; coating; impermeability test; concrete; crack

check for updates

Citation: Tan, B.; Qu, L.; Xia, Y.; Yang, X.; Su, B.; Wu, J.; Xiao, M. Experimental Study on Improving the Impermeability of Concrete under High-Pressure Water Environments Using a Polymer Coating. *Appl. Sci.* **2024**, *14*, 8507. https://doi.org/10.3390/app14188507

Academic Editor: Syed Minhaj Saleem Kazmi

Received: 22 August 2024
Revised: 19 September 2024
Accepted: 19 September 2024
Published: 21 September 2024

Copyright: © 2024 by the authors. Licensee MDPI, Basel, Switzerland. This article is an open access article distributed under the terms and conditions of the Creative Commons Attribution (CC BY) license (https://creativecommons.org/licenses/by/4.0/).

1. Introduction

As an important part of large-scale water conservancy projects, the safety of water conveyance tunnels is crucial. In China, increasing development scale and engineering challenges in hydropower are causing the concrete lining of water conveyance tunnels to permeate under high-pressure water. On the one hand, a water head of several hundred meters during tunnel operation will cause the concrete lining to crack, leading to internal water exosmosis [1–3]. On the other hand, during the emptying period of the tunnel, high-pressure external water in the surrounding rock will permeate the concrete lining in the opposite direction or directly permeate through cracks, leading to external water endosmosis [4,5]. Therefore, improving concrete impermeability is important for the safe operation of high-pressure water conveyance tunnels.

Concrete is a porous medium composed of cementitious materials, aggregates, and water in certain proportions. External water molecules continuously enter the interior

of concrete through convection, diffusion, and the capillary action of these pores. Water molecules under high pressure accelerate permeation into the concrete from the pore channel and change the parameters of the concrete, including the number of micropores, porosity, and pore size [6]. Researchers have found that high-pressure water can change the pore structure of concrete, reduce its strength, and increase its deformation [7–10]. This process reduces the bearing capacity of the structure. In addition, researchers have studied the effect of high water pressure on concrete cracking [11–13], finding that high-pressure water accelerates the cracking and failure process of concrete [14–16]. Therefore, an increasing number of researchers are paying attention to methods for improving concrete impermeability [17–20]. A common method is to mix additive agents with the concrete substrate to improve its pore structure [21,22]. Many studies have focused on the influence of the type and content of additive agents on concrete impermeability [23–25]. These studies have found that moderate additive agents can improve the overall density of concrete [18,26–32]. Additive agents inhibit water expansion in the internal pores of the concrete and enhance the strength of the concrete skeleton, thus improving the impermeability of the concrete itself. Additive agents can also reduce porosity and pore size to a certain extent, but they cannot change concrete's inherent hydrophilic properties. Water molecules under high water pressure can still permeate the interior of concrete through these pore channels. By contrast, dense and hydrophobic coatings are more effective in inhibiting the permeation of water molecules [33–36]. These coatings are polymer materials with no macroscopic pore channels inside, exhibiting excellent hydrophobicity and low permeability. Researchers have developed many hydrophobic coatings suitable for concrete. Gu et al. [37] designed a multi-layer coating with extremely strong hydrophobicity. At the same time, the coating also resists the permeation of chloride ions, with a 92% improvement over untreated concrete. Li et al. [38] prepared an inexpensive and environmentally friendly fluorine-free superhydrophobic coating based on carbon-based materials, with a water contact angle (WCA) of 156°. Ray et al. [39] modified the surface of concrete with silica sol and developed a hydrophobic coating suitable for high salt environments. In addition, researchers evaluated the impermeability of various coatings on the surface of concrete. Al-Kheetan et al. [40] studied the interaction between four coatings, namely, sodium acetate, fluoropolymer, silicone resin, and silane, and concrete with different moisture contents. They found that sodium acetate could provide optimal protection for concrete at various moisture contents. Alnushalam et al. [41] demonstrated that epoxy and polyurethane coatings performed better than acrylic, polymer, and chlorinated rubber coatings using the methods of water absorption, chloride permeability, and chloride diffusion.

At present, research on improving the impermeability of substrates with superhydrophobic coatings mainly focuses on the impermeability of coatings. There are few impermeability tests for coatings under high water pressure. It is worth noting that coatings exhibit varying impermeability in different high-pressure environments, which even lead to coating detachment or damage. On the one hand, microcracks are easily distributed on concrete surfaces under long-term high pressure [42]. This process requires the coating to have excellent mechanical properties. On the other hand, low interfacial strength causes coating blistering or delamination at the interface. Therefore, excellent interfacial strength is the foundation for coatings that provide effective protection for concrete [33,43,44]. The objectives of this study were to apply a coating to improve the impermeability of concrete in high-pressure water environments, and to study the seepage regulation of coated concrete and the failure mechanism of the SSS coating by conducting high-pressure impermeability tests. An SCU-SD-SP-II (SSS) coating was applied to the surface of concrete. The SSS coating formed a composite protective layer with the concrete interface through an epoxy-modified silicone (EMS) coating. We conducted high-pressure impermeability tests to study the seepage regulation of concrete and coated concrete in high-pressure environments. Subsequently, we designed impermeability tests with SSS coatings on the bottom and top surfaces of concrete specimens, simulating two working conditions of high-pressure water conveyance tunnels: internal water pressure during operation and external water pressure

during the emptying period. Considering the cracks on concrete surfaces in high-pressure environments, we also prepared natural cracks by splitting the concrete. We designed impermeability tests for SSS coatings on crack surfaces and analyzed the failure mechanism of SSS coatings in cracks. The experiments of this study considered high water pressure and concrete cracks, providing reference for impermeable tests in high-pressure water environments. The research results can solve the high-pressure seepage of concrete, which is significant for engineering economics and safety in global hydraulic engineering and ocean engineering.

2. Materials and Methods

2.1. SSS Coating and Preparation

The development of biomimetic materials has promoted research into surface-modified hydrophobic concrete [33]. The high WCA of this material type has a strong repulsive force against water. The SSS coating is a biomimetic functional coating that mainly consists of modified polydimethylsiloxane, which has good adhesion and weather resistance under conditions such as high-speed water flow, sand-carrying water flow, and a high-altitude climate. The performance parameters of the SSS coating are shown in Table 1.

Table 1. Performance parameters of the SSS coating.

Number	Performance Index	Parameter
1	Density	0.3–2.0 g/cm^3
2	Nominal fracture strength [1]	2.83 MPa
3	Real fracture strength [2]	18 MPa
4	Modulus	2–6 MPa
5	Elongation at break	20–700%
6	Water sliding angle (WSA)	5–30°
7	Water contact angle (WCA)	90–120°
8	Self-healing time	Visual self-healing within 1 min Functional self-healing 99% within 72 h
9	Operation life	≥10 years

[1] Nominal fracture strength is the ratio of the tensile strength to the initial cross-sectional area. [2] Real fracture strength is the ratio of the tensile strength to the actual cross-sectional area at fracture.

A composite protective layer constructed by placing a layer of primer between the coating and the substrate can enhance interfacial strength and provide concrete with long-term and effective protection [45]. To adapt to complex high-pressure water environments, we added a layer of the EMS coating between the SSS coating and concrete. EMS can promote the penetration of the SSS coating and react with it to form a composite protective layer with stronger adhesion ability, as shown in Figure 1a.

The preparation of the composite protective layer is shown in Figure 1b–e. The SSS coating is in a colorless and transparent flowing state. It is kept in a vacuum negative-pressure environment for 1–2 min to remove internal bubbles from the SSS coating. Subsequently, the SSS coating is slowly poured onto the concrete surface with the EMS coating attached. The uncured SSS coating has excellent flowability, can self-level within 5 min, and can cure itself within 24 h, ultimately forming a uniform thin layer with a thickness of about 0.5 mm on the surface.

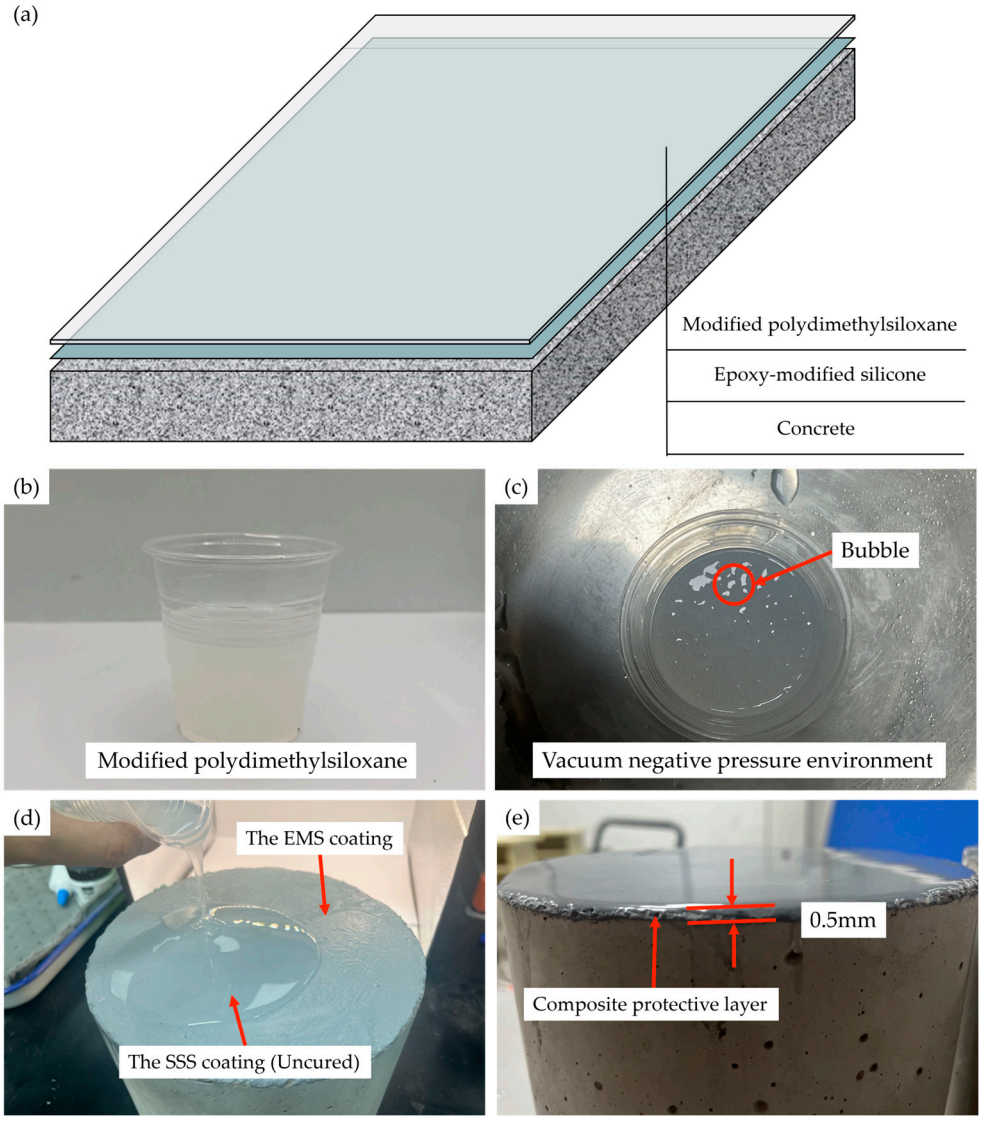


Figure 1. Composite protective layer and preparation. (**a**) Schematic diagram of the composite protective layer; (**b**–**e**) preparation of the composite protective layer.

2.2. Concrete and Specimens

Figure 2 shows the preparation process for concrete specimens. We poured circular cone concrete specimens according to GB/T 50082-2009 [46]. The height of the specimen was 150 mm, with a top diameter of 175 mm and a bottom diameter of 185 mm. The concrete grade was C30. According to GB50010-2010 [47], the standard compressive strength of C30 concrete cubes after 28 days of standard curing is 30 MPa, with a 95% guarantee rate. We used Sichuan Emeishan brand grade ordinary Portland cement (P.O 42.5) and F-class I grade fly ash as cementitious materials. Artificially crushed sand was used as fine aggregate (FA), with a fineness modulus and apparent density of 2.7 and 2660 kg/m^3, respectively. Figure 3a shows the grading curve of the sand. Continuous graded gravel was used as coarse aggregate (CA), and its particle size ranges and apparent density were 5–20 mm and 2740 kg/m^3, respectively. Figure 3b shows the grading curve of the gravel. The mix proportions are shown in Table 2, and the unit quantities are shown in Table 3.

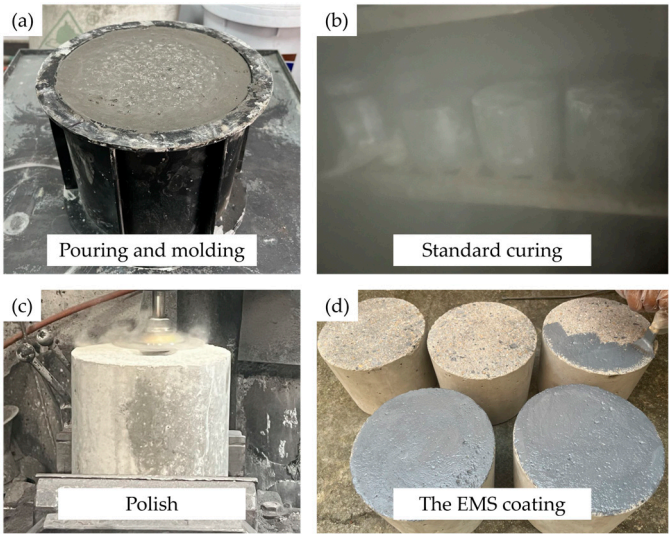


Figure 2. Preparation process for concrete specimens. (**a**) Pouring and molding of concrete samples; (**b**) standard curing of the concrete according to GB50010-2010; (**c**) polishing of the surface of the concrete; (**d**) application of the EMS coating.

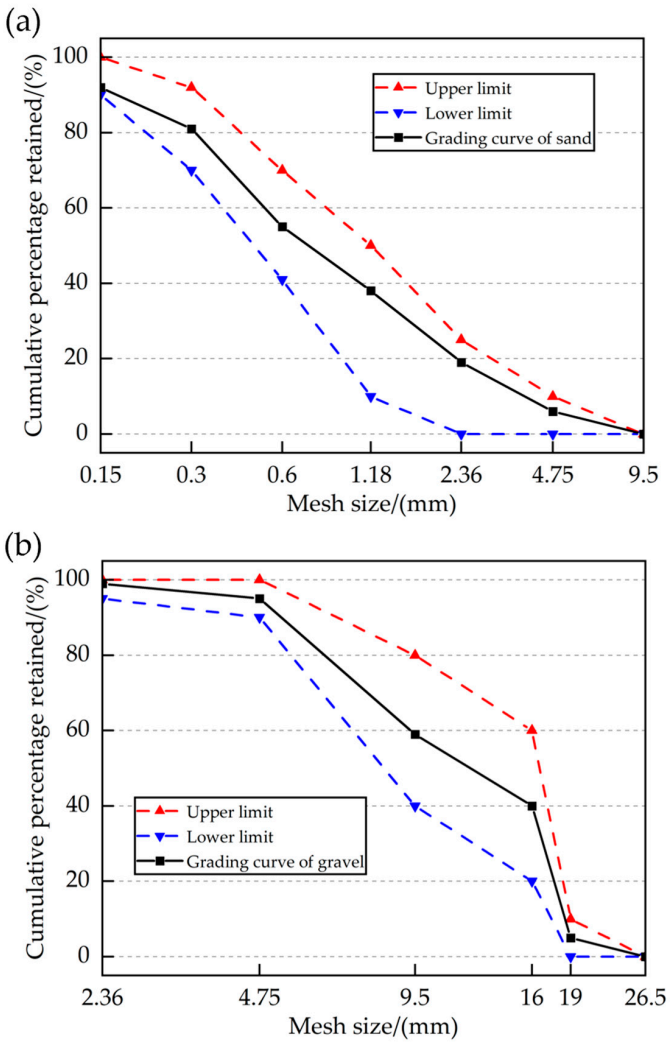


Figure 3. Grading curve of FA and CA. (**a**) Grading curve of sand and its grading limit; (**b**) grading curve of gravel and its grading limit.

Table 2. Mix proportion.

Water–Binder Ratio	Fly Ash	Water-Reducing Admixture	Percentage of Sand
0.43	25%	0.25%	40%

Table 3. Unit quantity (kg/m^3).

Water	Cement	Fly Ash	Water-Reducing Admixture	Sand	Gravel
186	323	108	1.08	603	904

Good adhesion effectively ensures the protection of concrete by the coating. Studies have found that adhesion force is related to the properties of the coating and primer, as well as the surface roughness of the substrate [48–50]. However, the quality of the concrete surface often leads to coating detachment. The failure mode that usually occurs in interface strength tests is mainly concrete failure [51,52]. The surface layer of concrete is a cement layer without coarse aggregates, and its density and strength are lower than the aggregate layer inside the concrete. In this study, the optimal adhesion scheme was to use the EMS as the primer and polish the concrete surface. Therefore, we used a polishing machine to polish the surface of the concrete specimen after curing. This step removed the cement layer from the surface (Figure 2c) and exposed the aggregate layer. The EMS coating was applied to the polished aggregate layer (Figure 2d).

2.3. Experimental Design and Groups

To study the impermeability performance of the SSS-coated concrete in a high-pressure environment, we set up three experimental groups to simulate different working conditions. The experimental groups and parameters are shown in Table 4. A schematic diagram and physical images of the experimental groups are shown in Figure 4. Experimental group C-O-S_1 was used to study the concrete and coated concrete seepage regulation. For comparison, concrete without anti-seepage treatment, concrete coated with waterproofing agents, and SSS-coated concrete were selected to conduct 24 h impermeability tests under water pressures of 1 MPa, 2 MPa, and 3 MPa. The waterproofing agents were permeable organic sodium silicates available on the market. The SSS coating thickness was 0.5 mm. Experimental group S_1-S_2 simulated two working conditions: the internal water pressure during the operation period of the high-pressure water conveyance tunnel and the external water pressure during the emptying period. The SSS coating was applied to the top and bottom surfaces of the specimen, simulating the external and internal water working conditions, respectively. The SSS coating thickness was 0.5 mm, and impermeability tests were conducted for 10, 20, and 30 days under a water pressure of 3 MPa. Finally, to study the effect of concrete cracks in high-pressure water environments on the impermeability of the SSS coating, impermeability tests were conducted on surfaces with different crack widths in experimental group SC_1-SC_2. We prepared natural cracks through splitting and controlled the width of the cracks using longitudinal splitting and lateral splitting. During longitudinal splitting, steel bars were placed on the bottom and top surfaces of the specimen. Due to the influence of the steel bars' diameter, wide cracks appeared on the bottom surface of the specimen after splitting, with widths ranging from 2 mm to 5 mm. During lateral splitting, the steel bars were placed on both sides of the specimen; after splitting, thin cracks appeared on the bottom of the specimen with a width of less than 1 mm. The bottom surface of the split specimen was coated with the SSS coating with a thickness of 1 mm. The specimen was loaded in stages of 0.5 MPa per level. If the SSS coating was damaged during the pressurization process, i.e., water seeped from the top surface of the specimen, the specimen was immediately removed. After the water pressure

was increased to the design water pressure, if there was no water seepage on the top surface of the specimen, the specimen was removed after 24 h of stabilization.

Table 4. Experimental groups and parameters.

Number	Group	Crack Width (mm)	Water Pressure (MPa)	Pressurization Time	Number of Specimens
1	C-O-S_1	0	1	1 d	3
2	C-O-S_1	0	2	1 d	3
3	C-O-S_1	0	3	1 d	3
4	S_1-S_2	0	3	10 d	3
5	S_1-S_2	0	3	20 d	3
6	S_1-S_2	0	3	30 d	3
7	SC_1-SC_2	2–5	1	/	3
8	SC_1-SC_2	2–5	2	/	3
9	SC_1-SC_2	2–5	3	/	3
10	SC_1-SC_2	<1	3	/	3

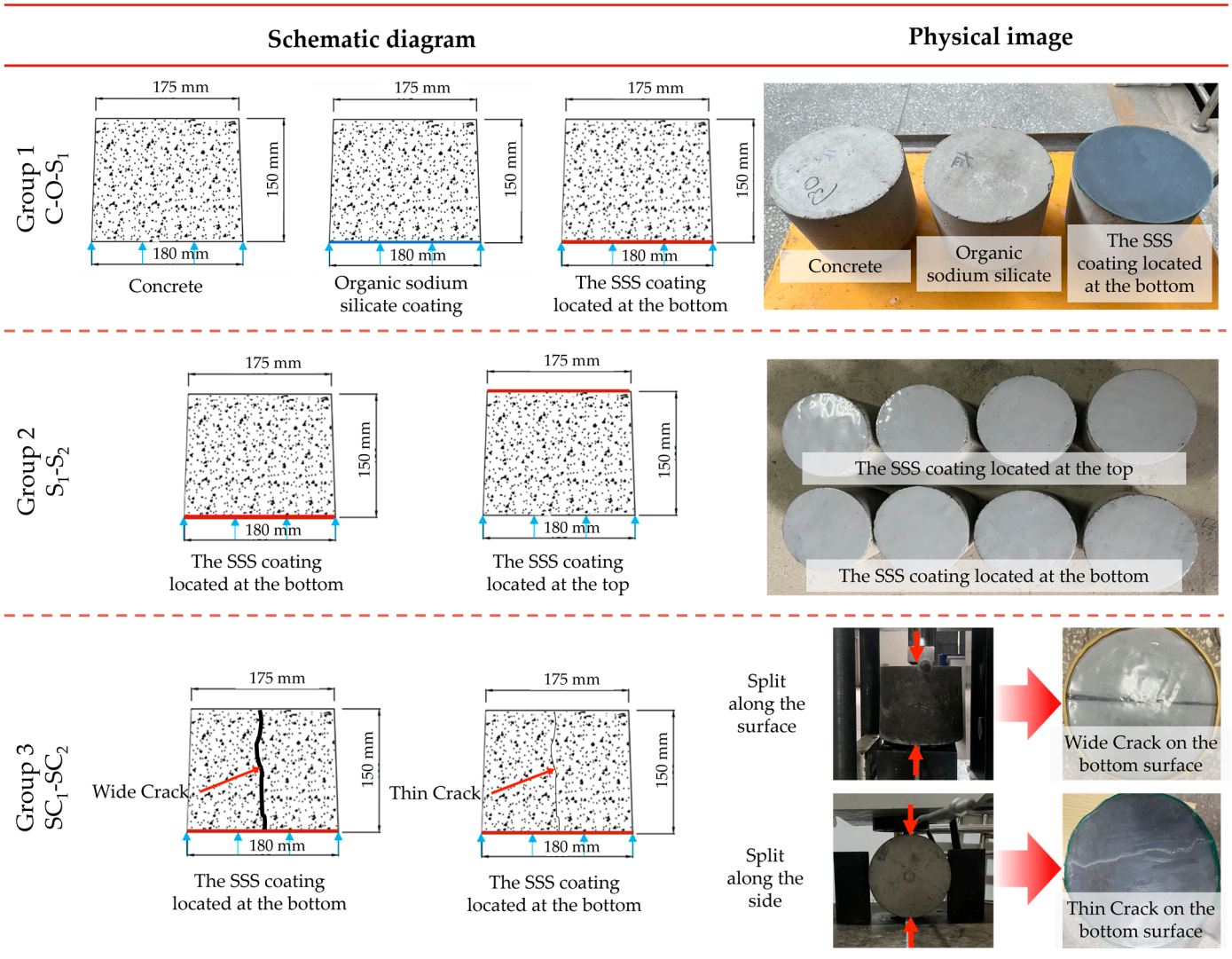


Figure 4. A schematic diagram and physical images of the experimental groups. (Note: the blue arrows represent the direction of high-pressure water.)

2.4. Test Method

This study used the HP-4.0 permeameter for uniaxial hydraulic loading on conical concrete specimens according to GB/T 50082-2009 [46]. The average seepage height and relative permeability coefficient of concrete under constant water pressure were measured to indicate concrete impermeability. The experiment was conducted indoors at a temperature of 20 ± 2 °C and a humidity of 50 ± 10%. The experimental instruments included concrete specimens, a press machine, an HP-4.0 permeameter (Hebei Better United Test Equipment Co., Ltd., Hebei, China), and rubber used for sealing. Figure 5 shows the process of the impermeability test. Before loading, the specimen side was sealed with rubber. Subsequently, the specimen was pressed into the steel mold by the press machine and was loaded into the HP-4.0 permeameter. After the experiment, the specimen was split with two steel bars on the press. We traced the seepage marks with a red pen and measured the height of 10 points at equal intervals along the marks with a vernier caliper. The seepage height of a specimen was calculated according to Formula (1):

$$\overline{h} = \frac{1}{10}\sum_{1}^{10} h_i \tag{1}$$

where $\overline{h}$ is the seepage height of a specimen, and h_i is the seepage height of the ith position.

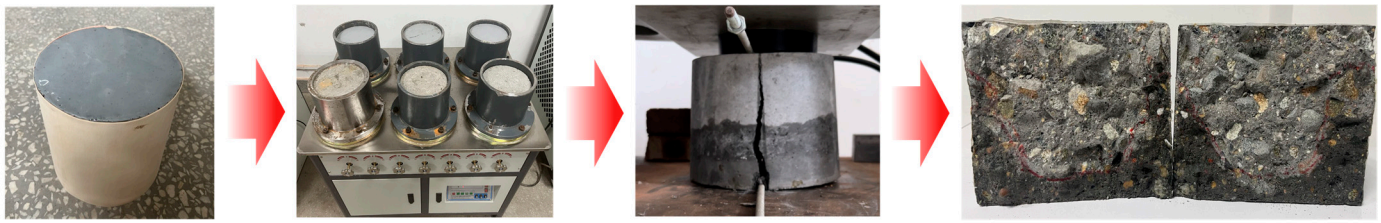


Figure 5. The impermeability test process.

The average value of $\overline{h}$ from three specimens in each experiment is taken as the average seepage height. According to SL 352-2006 [53], the relative permeability coefficient of the concrete impermeability test can be calculated from the average seepage height. The relative permeability coefficient is calculated according to Formula (2):

$$K_r = \frac{aD_m{}^2}{2TH} \tag{2}$$

where K_r is the relative impermeability coefficient of concrete (m/s); D_m is the average seepage height (mm); H is the water pressure expressed in millimeters, representing the height of the water column (mm); T is the pressurization time (s); and a is the water absorption rate of concrete, taking the conventional rate of $a = 0.03$.

3. Results and Analysis

3.1. Test Results of Concrete and Coated Concrete

The average seepage height and relative permeability coefficient of the three types of concrete in experimental group are shown in Figure 6. During 24 h of continuous loading, as the water pressure increases, the average seepage height of the concrete and the concrete coated with organic sodium silicate increases, indicating that high pressure accelerates water permeation into concrete. However, the relative permeability coefficient decreases with increasing water pressure. The reason for this is that high-pressure water enters the interior of the concrete, which improves the overall compactness of the concrete. The water pressure rapidly decays along the seepage channel, reducing water permeability; however, the permeation of water cannot be completely prevented. By comparing the

impermeability performance of concrete and the concrete coated with organic sodium silicate, it is found that organic sodium silicate can reduce the average seepage height and relative permeability coefficient by 35.5% and 58.3%, respectively, under the same water pressure. When sodium organic silicate comes into contact with carbon dioxide in the air, methylsilicol is generated, blocking the pores in the concrete and enhancing its impermeability. The average seepage height of the SSS-coated concrete is 0 mm, indicating that water under a maximum pressure of 3 MPa cannot penetrate the SSS coating within 24 h. Compared with porous and permeable concrete, dense and hydrophobic coatings have a very low permeability coefficient and strong repulsion against pressurized water, which can completely isolate high-pressure water in a short period of time.

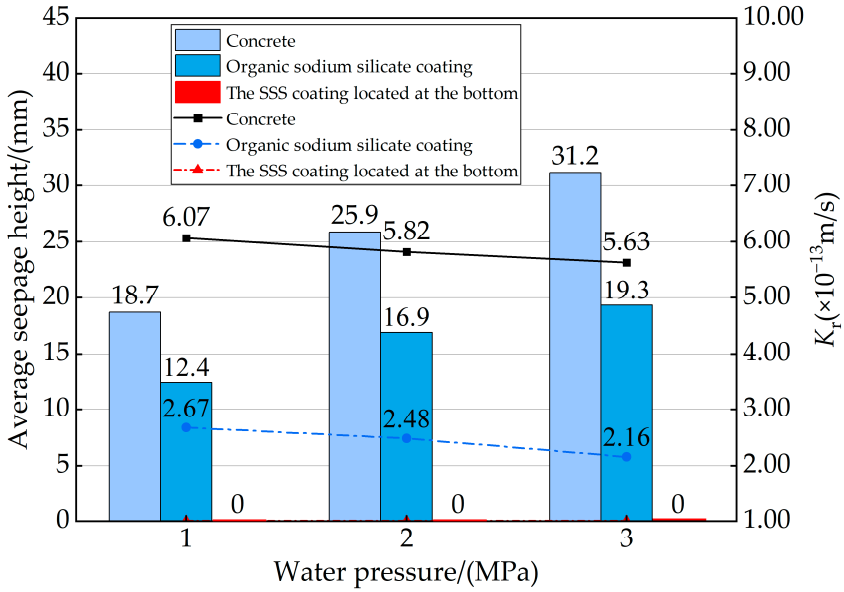


Figure 6. The average seepage height and relative permeability coefficient of group C-O-S_1.

3.2. Test Results of Internal and External Water Pressure in the Water Conveyance Tunnel

In experimental group S_1-S_2, the SSS coating was placed on the bottom or top surface of the specimen. The average seepage height and relative permeability coefficients are shown in Figure 7. Regardless of whether the SSS coating was on the bottom or top surface, the specimens were permeable under a long-term water pressure of 3 MPa. With an increase in time, the average water seepage height of the specimens coated on the bottom surface and those coated on the top surface increased. However, the relative permeability coefficient of the former increased, while that of the latter decreased. This result occurred because the two permeation mechanisms are different. When the SSS coating is on the bottom surface of the specimen, high-pressure water must pass through the SSS coating before entering the concrete. The SSS coating acts as a barrier with an ultra-low permeability coefficient, isolating water permeation. Therefore, the permeability coefficient is relatively low in the early stages of permeation. In the later stages of permeation, high-pressure water enters the concrete, showing a relatively high permeability coefficient. When the SSS coating is on the top surface, high-pressure water directly enters the concrete, and the seepage regulation is the same as that of concrete and the concrete coated with organic sodium silicate, as shown in Figure 6. However, the relative permeability coefficient is much smaller. The SSS coating improves the airtightness of the concrete, resulting in the pores' inability to release gases. As high-pressure water enters the pore channel, the pore pressure inside the channel increases, balancing the pore water pressure and inhibiting further water permeation. In summary, the SSS coating on the top surface of the specimen indirectly enhances concrete impermeability. By contrast, the SSS coating on the specimen's bottom surface directly prevents water permeation. The average penetration height and

relative permeability coefficient of the specimens coated on the bottom surface decreased by 49.6% and 71.2%, respectively, compared with those of the specimens coated on the top surface. This finding indicates that the direct waterproofing effect of the SSS coating positively affects concrete impermeability.

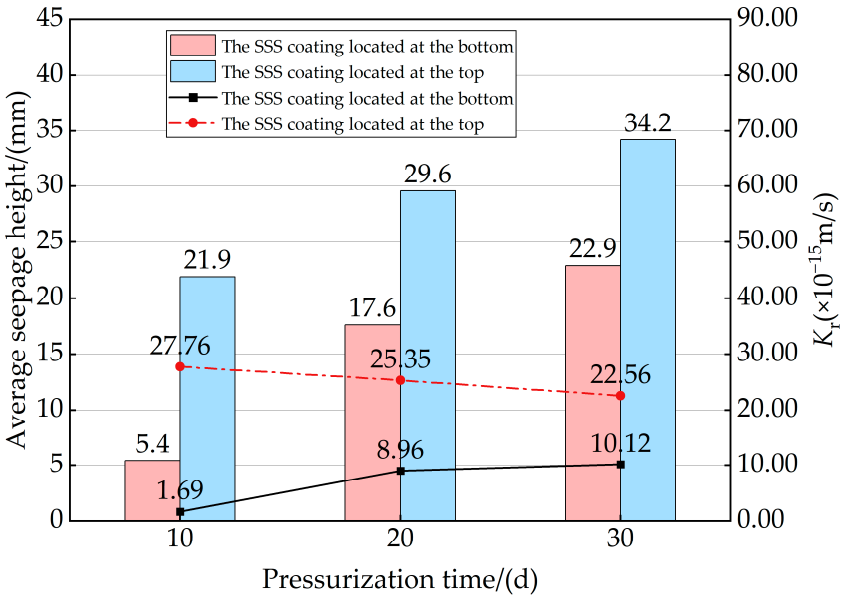


Figure 7. The average seepage height and relative permeability coefficient of group S_1-S_2.

3.3. Test Results of the SSS Coating on the Surface of Concrete Cracks

The impermeability test results of the three SSS-coated specimens with cracks were the same in each experiment, as shown in Figure 8. The impermeability of the SSS coating after concrete cracking is related to the crack width and water pressure. When the crack width is 2–5 mm and the water pressure is increased to 1 MPa, there is no water seepage on the top surface of the specimen. After 24 h of water pressure loading, the specimen is removed, and the SSS coating on the bottom of the specimen is relatively flat. The SSS coating has a depression at the crack, but no damage occurs. When the crack width is 2–5 mm and the water pressure is increased to 2 MPa, a small amount of water seeps out from the top surface of the specimen, and the SSS coating on the bottom surface of the specimen bubbles and seeps at the edge of the crack. This finding indicates that the SSS coating has been damaged. When the crack width is 2–5 mm and the water pressure is increased to 3 MPa, a large amount of water seeps out of the top surface of the specimen. The concrete on both sides of the crack shifts due to water pressure, causing the SSS and EMS coatings to detach from the concrete and tear. When the crack width is less than 1 mm, the flatness of the bottom surface of the specimen is high, and there are no obvious concave areas. The water pressure is increased to 3 MPa, and after 24 h of water pressure loading, the specimen is removed. The SSS coating is locally damaged, and there is no water seepage on the inner surface of the specimen, indicating that the SSS coating still has impermeability.

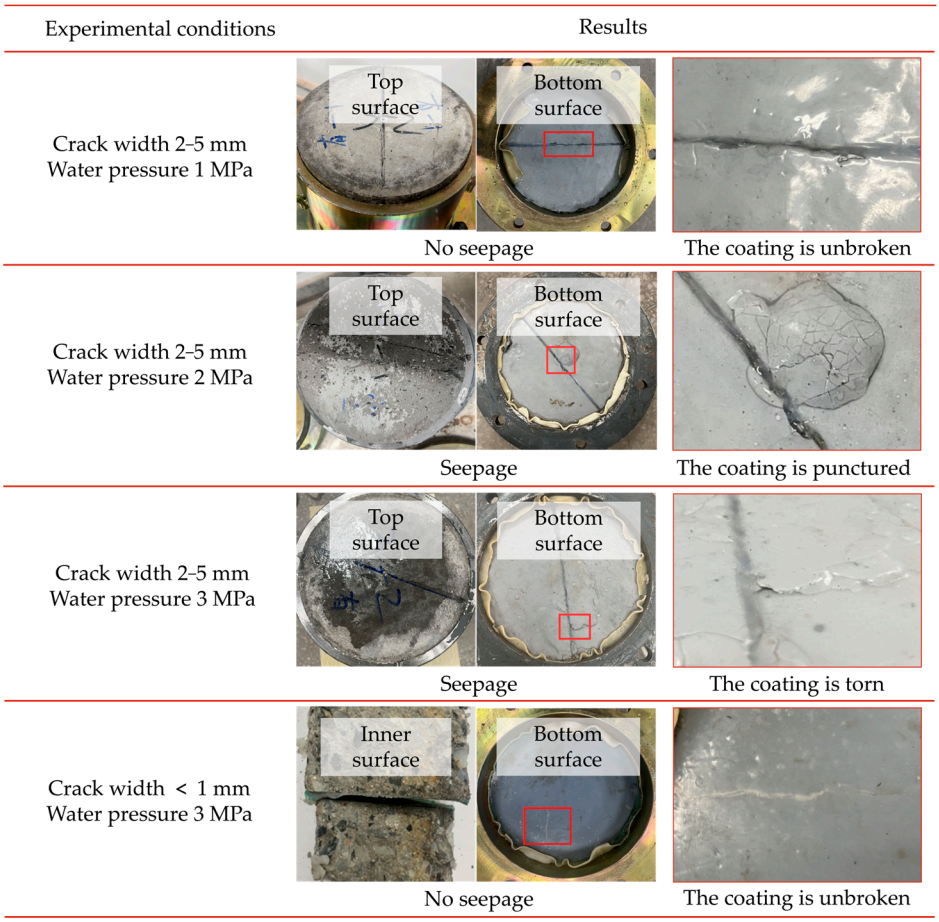


Figure 8. The results of the SSS coating under different concrete crack widths.

4. Discussion

The hydrophobicity of the SSS coating can effectively improve the impermeability of concrete under high water pressure. The impermeability of coated concrete is influenced by multiple factors based on the experimental results. These factors include pore structure, water pressure, time, direction of water penetration, and crack width. As the water pressure increases, the depth of water seepage in the concrete also increases. During this process, water pressure changes the pore structure of the concrete. Dong et al. [32] pointed out the relationship between porosity and the relative permeability coefficient. Feng et al. [17] conducted permeability tests at 0 MPa, 1.4 MPa, and 2.4 MPa. Due to the low water pressure during the initial loading, the relative permeability coefficient of concrete first increased and then decreased. This study started from 1 MPa and the relative permeability coefficient continued to increase. It can be seen that a water pressure of 1 MPa is a condition for reducing the relative permeability coefficient of concrete. After the water pressure has been applied for a long time, the SSS coating and concrete are eventually penetrated. Whether in coatings or concrete, the permeation does not stop. Jalilian et al. [54] and Wang et al. [55] also verified this by calculating the weight loss rate of the coating and measuring the long-term water absorption rate of concrete, respectively. This study does not consider coating thickness, which is also an important factor in slowing down the penetration rate. The potential future exploration is the relationship between coating thickness and penetration rate. This is significant for determining the engineering quantity of coatings. When the coating is not on the concrete-facing surface, water enters the concrete from the other side. The SSS coating can indirectly reduce the impermeability of concrete by improving its airtightness. Zheng et al. [56] developed a silicone polymer coating that improved airtightness. Penetration testing showed that it reduced the gas permeability of concrete by 40–70%. This study also focuses on the damage of coatings in high-pressure

water environments. Coating damage is related to water pressure and crack width. The main types of damage are puncture damage and tear damage.

4.1. Puncture Damage

Figure 9 shows the puncture damage process of the SSS coating. The puncture damage is mainly caused by stress concentration at the crack tip during heavy deformation of the SSS coating. After cracks appear on the concrete surface, the initial crack width is less than 1 mm, the concrete surface is relatively flat, and the SSS coating cannot be punctured. As the crack width exceeds 1 mm, the effect of water pressure causes the SSS coating to extend toward the inside of the crack. When the tensile stress at the interface exceeds the interface strength, the SSS coating separates from the concrete. As the SSS coating deforms, stress concentration occurs at the crack tip. When the tensile stress exceeds the SSS coating strength, the SSS coating is punctured and loses its impermeability. High-pressure water enters the crack interior. After the external water recedes, the SSS coating self-heals and locks the water in the cracks. The separated coating cannot recover after deformation, forming bubbles with water.

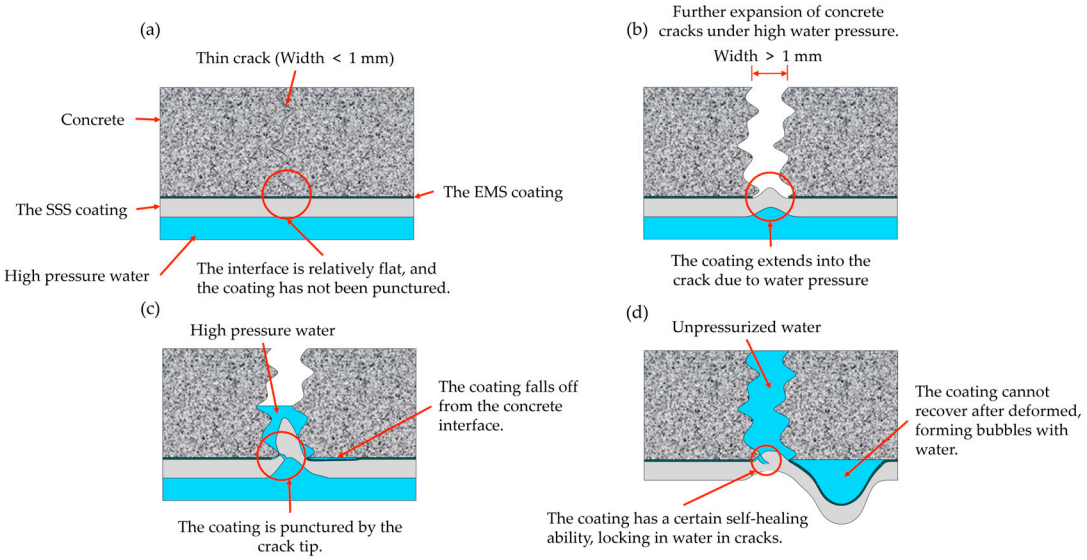


Figure 9. The process of puncture damage. (**a**) The crack width is less than 1 mm, and the coating has not been punctured; (**b**) When the crack width exceeds 1 mm, the coating extends; (**c**) The coating is punctured due to stress concentration; (**d**) The coating self-heals under low pressure.

4.2. Tear Damage

Figure 10 shows the tear damage process of the SSS coating. Tear damage is mainly caused by the stress concentration of the SSS coating at the tearing point during uneven concrete settlement. After the appearance of cracks on the concrete surface, the initial crack width is less than 1 mm, the concrete surface is flat, and there is no displacement on either side of the crack. As the crack width exceeds 1 mm, the water pressure causes the SSS coating to extend toward the inside of the crack. As the water pressure increases, the concrete on both sides of the crack moves, causing the SSS coating to separate from the concrete at the crack tip. As the displacement distance of the concrete on both sides of the crack increases, the SSS coating, along with the EMS coating, is torn apart along the interface. The EMS coating is harder and much thinner than the SSS coating. Therefore, stress concentration occurs at the tip of the EMS coating where the SSS coating tears. When the tensile stress exceeds the SSS coating strength, the SSS coating is punctured and loses its impermeability. Due to the tearing effect, the rupture port of the SSS coating is further torn apart, and the SSS coating loses its self-healing ability. Large amounts of high-pressure water enter cracks, causing severe water seepage.

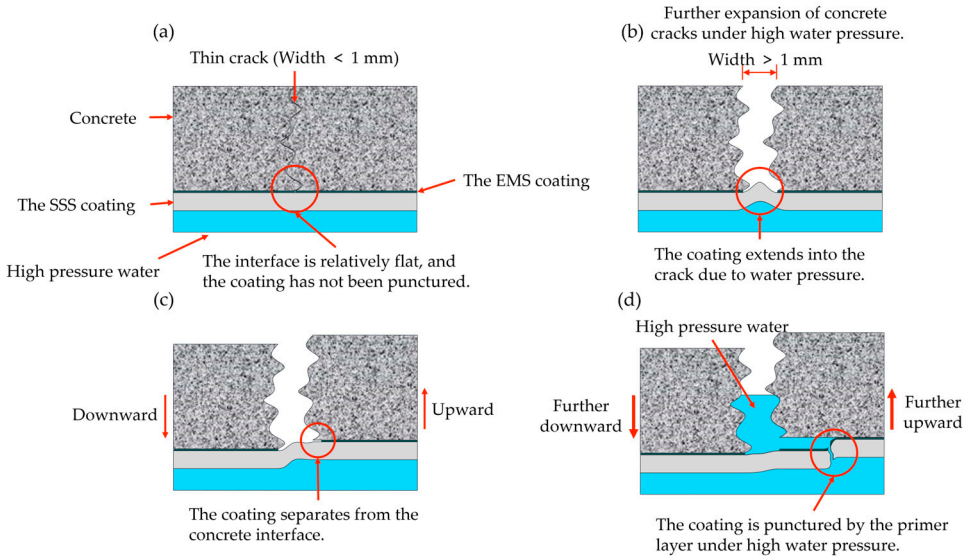


Figure 10. The process of tear damage. (**a**) The crack width is less than 1 mm, and the coating has not been punctured; (**b**) When the crack width exceeds 1 mm, the coating extends; (**c**) The coating falls off due to concrete displacement; (**d**) The coating is punctured by the primer.

5. Conclusions

This study applied a polymer coating known as SSS coating to concrete surfaces in order to improve their impermeability in high-pressure water environments. A series of impermeability tests were conducted to analyze the seepage regulation of the coated concrete and the failure mechanism of the coating after concrete cracking. The following conclusions can be drawn from the experimental results:

(1) The EMS coating promoted the permeation of the SSS coating and reacted with the uncured coating to form a composite protective layer. This process increased the adhesion of the SSS coating to the concrete. Moreover, the SSS coating did not separate from the concrete surface without cracks under a water pressure of 3 MPa.

(2) As the water pressure increased, the average seepage height of the concrete also increased. High pressure also increased concrete compactness, resulting in a decrease in the concrete's relative permeability coefficient. Organic sodium silicate could improve the pore structure of the concrete, reducing the average seepage height and relative permeability coefficient of concrete by 35.5% and 58.3%, respectively, under the same water pressure. The SSS coating effectively improved the impermeability of concrete. The SSS-coated concrete was not penetrated, indicating that 3 MPa pressurized water cannot penetrate the SSS coating with a thickness of 0.5 mm within 24 h.

(3) As the water pressure time increased, the average seepage height of the SSS-coated concrete increased, indicating that the SSS coating was ultimately penetrated by water. The impermeability of the SSS coating varies in different directions in contact with water. The SSS coating located on the top surface of the specimen indirectly enhanced the impermeability of the concrete. The SSS coating located on the bottom surface of the specimen directly prevented permeation. Compared with the former, the average seepage height and relative permeability coefficient of the latter decreased by 49.6% and 71.2%, respectively.

(4) The impermeability of the SSS coating after concrete cracking is related to crack width and water pressure. When the crack width was less than 1 mm, the SSS coating could maintain impermeability under a water pressure of 3 MPa. When the crack width was greater than 2 mm and the water pressure was 1 MPa, the SSS coating deformed. As the water pressure increased, the SSS coating was punctured or torn due to stress concentration.

This study focused on the effects of high-pressure water and crack width on the impermeability of the coating, and changes in coating thickness and crack number are also potential future directions. The research results can be applied to global hydraulic engineering and ocean engineering, which is beneficial for improving the service life of concrete in high-pressure water environments and is significant for engineering economics and safety.

Author Contributions: Conceptualization, B.T. and L.Q.; methodology, L.Q. and M.X.; validation, B.T., L.Q. and Y.X.; formal analysis, B.T. and L.Q.; investigation, Y.X. and X.Y.; data curation, B.S.; writing—original draft preparation, L.Q.; writing—review and editing, B.T.; visualization, J.W.; supervision, X.Y.; funding acquisition, M.X. All authors have read and agreed to the published version of the manuscript.

Funding: This study was financially supported by the Natural Science Foundation of Sichuan Province, China (No. 2024NSFSC0836) and the National Natural Science Foundation of China (No. 52109135).

Institutional Review Board Statement: Not applicable.

Informed Consent Statement: Not applicable.

Data Availability Statement: The original contributions presented in the study are included in the article. Further inquiries can be directed to the corresponding authors.

Acknowledgments: We would like to thank Shihua Dong for providing technical support. We would also like to express our gratitude to POWERCHINA Sinohydro Bureau 5 Corporation Limited for their assistance.

Conflicts of Interest: Authors Baobao Tan and Bo Su were employed by the company Guoneng Sichuan Ashui Power Development Corporation Limited. Authors Yong Xia and Xingyi Yang were employed by the company POWERCHINA Chengdu Engineering Corporation Limited. The remaining authors declare that the re-search was conducted in the absence of any commercial or financial relationships that could be construed as a potential conflict of interest.

References

1. Bian, K.; Liu, J.; Xiao, M.; Liu, Z. Cause investigation and verification of lining cracking of bifurcation tunnel at Huizhou Pumped Storage Power Station. *Tunn. Undergr. Space Technol.* **2016**, *54*, 123–134. [CrossRef]
2. Yang, F.; Zhang, C.; Zhou, H.; Liu, N.; Zhang, Y.; Azhar, M.U.; Dai, F. The long-term safety of a deeply buried soft rock tunnel lining under inside-to-outside seepage conditions. *Tunn. Undergr. Space Technol.* **2017**, *67*, 132–146. [CrossRef]
3. Wang, D.; Zhu, H.; Huang, J.; Yan, Z.; Zheng, X.; Shi, B. Fiber optic sensing and performance evaluation of a water conveyance tunnel with composite linings under super-high internal pressures. *J. Rock Mech. Geotech. Eng.* **2023**, *15*, 1997–2012. [CrossRef]
4. Tan, Y.; Smith, J.V.; Li, C.-Q.; Currell, M.; Wu, Y. Predicting external water pressure and cracking of a tunnel lining by measuring water inflow rate. *Tunn. Undergr. Space Technol.* **2018**, *71*, 115–125. [CrossRef]
5. Li, Z.; Chen, Z.; He, C.; Chen, K.; Zhang, H.; Ma, C.; Li, X.; Liu, M. Experimental simulation of seepage field distribution for small interval tunnel under varying-head infiltration. *Transp. Geotech.* **2023**, *41*, 101029. [CrossRef]
6. Zhang, G.; Zheng, H.; Wei, X.; Li, Z.; Yan, Z.; Chen, X. Concrete mechanical properties and pore structure influenced by high permeability water pressure. *Dev. Built Environ.* **2024**, *17*, 100385. [CrossRef]
7. Muhaimin, A.A.; Adel, M.; Nagai, K. Investigating the Effect of Repeated High Water Pressure on the Compressive and Bond Strength of Concrete with/without Steel Bar. *Materials* **2021**, *14*, 527. [CrossRef]
8. Wang, Q.; Liu, Y.; Peng, G. Effect of water pressure on mechanical behavior of concrete under dynamic compression state. *Constr. Build. Mater.* **2016**, *125*, 501–509. [CrossRef]
9. Haynes, H.H.; Highberg, R.S. Concrete Properties at Ocean Depths. *J. Waterw. Harb. Coast. Eng. Div.* **1976**, *102*, 455–470. [CrossRef]
10. Zhou, J.; Zhao, X.; Nie, Y.; Tian, Y. Influence of High Water Pressure on Static and Dynamic Compressive Strength of Concrete. *Adv. Civ. Eng.* **2020**, *2020*, 8814626. [CrossRef]
11. Zhong, H.; Li, H.; Ooi, E.T.; Song, C. Hydraulic fracture at the dam-foundation interface using the scaled boundary finite element method coupled with the cohesive crack model. *Eng. Anal. Bound. Elem.* **2018**, *88*, 41–53. [CrossRef]
12. Barpi, F.; Valente, S. The cohesive frictional crack model applied to the analysis of the dam-foundation joint. *Eng. Fract. Mech.* **2010**, *77*, 2182–2192. [CrossRef]
13. Hou, S.; Li, K.; Hu, X.; Shi, C. Exploring the nonlinear behavior of flow through cracked concrete by water permeability test. *Cem. Concr. Compos.* **2024**, *150*, 105557. [CrossRef]

14. Tian, Y.; Zhao, X.; Zhou, J.; Nie, Y. Investigation on the influence of high-pressure water environment on fracture performance of concrete. *Constr. Build. Mater.* **2022**, *341*, 127907. [CrossRef]
15. Tian, Y.; Zhao, X.; Tai, Y.; Chen, Y.; Zhou, J. Crack extension at the concrete–rock interface damaged by high-pressure water environment: DIC research. *Theor. Appl. Fract. Mech.* **2023**, *126*, 103966. [CrossRef]
16. Tian, Y.; Zhao, X.; Tai, Y.; Chen, Y.; Zhou, J. Investigation on the fracture toughness of concrete-rock interface damaged by high-pressure water environment. *Eng. Fract. Mech.* **2023**, *277*, 109025. [CrossRef]
17. Feng, K.; Pan, J.; Xing, W.; Li, M.; Geng, J.; He, C. Experimental study on the high water pressure erosion mechanism and its influence on the submarine shield tunnel concrete segments. *Constr. Build. Mater.* **2023**, *408*, 133577. [CrossRef]
18. Muhammad, N.Z.; Keyvanfar, A.; Majid, M.Z.A.; Shafaghat, A.; Mirza, J. Waterproof performance of concrete: A critical review on implemented approaches. *Constr. Build. Mater.* **2015**, *101*, 80–90. [CrossRef]
19. Zhang, H.; Wang, H.; Zhou, Y.; Chang, Z. Waterproofing performance of polypropylene—Concrete wall of underground silo under combined compressive stress and water pressure. *Heliyon* **2022**, *8*, e12074. [CrossRef]
20. He, X.; Guo, X.; Li, S.; Xu, G. Experimental study on impermeability of concrete lining joint. *IOP Conf. Ser. Earth Environ. Sci.* **2019**, *304*, 052034. [CrossRef]
21. Bohus, S.; Drochytka, R.; Taranza, L. Fly-ash usage in new cement-based material for concrete waterproofing. *Adv. Mater. Res.* **2012**, *535–537*, 1902–1906. [CrossRef]
22. Ramli, M.; Tabassi, A.A.; Porosity, K.; Hoe, W. Porosity, pore structure and water absorption of polymer-modified mortars: An experimental study under different curing conditions. *Compos. Part B Eng.* **2013**, *55*, 221–233. [CrossRef]
23. Plaza, P.; del Bosque, I.F.S.; Sánchez, J.; Medina, C. Recycled Eco-Concretes Containing Fine and/or Coarse Concrete Aggregates. Mechanical Performance. *Appl. Sci.* **2024**, *14*, 3995. [CrossRef]
24. Dvorkin, L.; Bordiuzhenko, O.; Mierzwiński, D.; Tracz, T.; Sitarz, M. Water Impermeability of Self-Compacting Fly-Ash-Containing Concrete. *Appl. Sci.* **2024**, *14*, 5373. [CrossRef]
25. Voit, K.; Zeman, O.; Janotka, I.; Adamcova, R.; Bergmeister, K. High-Durability Concrete Using Eco-Friendly Slag-Pozzolanic Cements and Recycled Aggregate. *Appl. Sci.* **2020**, *10*, 8307. [CrossRef]
26. Yang, W.; Tang, Z.; Wu, W.; Zhang, K.; Yuan, J.; Li, H.; Feng, Z. Effect of different fibers on impermeability of steam cured recycled concrete. *Constr. Build. Mater.* **2022**, *328*, 127063. [CrossRef]
27. Zhang, Y.; Zhou, G.; Zheng, Y. Effect of fiber type on the mechanical properties and durability of hardened concrete. *J. Mater. Sci.* **2023**, *58*, 16063–16088. [CrossRef]
28. Xu, Y.; Cui, L.; Yuan, Q.; Huang, C. Impermeability test on carbon fibre reinforced concrete. *Chem. Eng. Trans.* **2018**, *66*, 1075–1080.
29. Yang, W.; Huang, Y.; Tang, Z.; Xiong, X.; Li, C.; Zhong, X.; Liu, L.; Zhou, H.; Zhang, X. Impermeability performance and corrosion resistance mechanism of basalt fiber recycled concrete under the coastal tidal environment. *Constr. Build. Mater.* **2024**, *411*, 134510. [CrossRef]
30. Qi, F.; Wu, Y.X.; Zhang, W.J. Study on Fiber Concrete Impermeability Test and its Application in Subway Station. *Adv. Mater. Res.* **2011**, *261–263*, 280–286. [CrossRef]
31. Hu, Q.; Yang, C.; Zhang, K.; Wang, X.; Wang, W.; Liu, Y.; Li, Z.; Ma, G.; Jiang, L. Study on the impermeability of recycled aggregate thermal insulation concrete. *J. Build. Eng.* **2023**, *77*, 107400. [CrossRef]
32. Dong, D.; Huang, Y.; Gao, X.; Bian, Y.; Zhu, J.; Hou, P.; Chen, H.; Zhao, P.; Wang, S.; Lu, L. Effect of polyvinyl alcohol powder on the impermeability, frost resistance and pore structure of calcium sulfoaluminate cement concrete. *Constr. Build. Mater.* **2023**, *409*, 133858. [CrossRef]
33. Wu, Y.; Dong, L.; Shu, X.; Yang, Y.; She, W.; Ran, Q. A review on recent advances in the fabrication and evaluation of superhydrophobic concrete. *Compos. Part B Eng.* **2022**, *237*, 109867. [CrossRef]
34. Antolín-Rodríguez, A.; Merino-Maldonado, D.; González-Domínguez, J.M.; Fernández-Raga, M.; Pozo, J.M.M.-D.; García-González, J.; Juan-Valdés, A. Performance of graphene oxide as a water-repellent coating nanomaterial to extend the service life of concrete structures. *Heliyon* **2024**, *10*, e23969. [CrossRef] [PubMed]
35. Thissen, P.; Bogner, A.; Dehn, F. Surface treatments on concrete: An overview on organic, inorganic and nano-based coatings and an outlook about surface modification by rare-earth oxides. *RSC Sustain.* **2024**, *2*, 2092–2124. [CrossRef]
36. Vipulanandan, C.; Liu, J. Performance of Coated Concrete in Wastewater Environment. *Pipeline Eng. Constr.* **2012**, *713*, 1–11. [CrossRef]
37. Gu, W.; Liu, R.; Zhang, Y.; Yu, X.; Feng, P.; Ran, Q.; Zhang, Y.; Zhang, Y. Robust water-borne multi-layered superhydrophobic coating on concrete with ultra-low permeability. *Constr. Build. Mater.* **2024**, *411*, 134573. [CrossRef]
38. Li, Y.; Gou, L.; Wang, H.; Wang, Y.; Zhang, J.; Li, N.; Hu, S.; Yang, J. Fluorine-free superhydrophobic carbon-based coatings on the concrete. *Mater. Lett.* **2019**, *244*, 31–34. [CrossRef]
39. Ray, S.S.; Peddinti, P.R.T.; Soni, R.; Kim, B.; Park, Y.-I.; Kim, I.-C.; Lee, C.Y.; Kwon, Y.-N. Effectiveness of nanoparticles-based ultrahydrophobic coating for concrete materials. *J. Build. Eng.* **2023**, *66*, 105799. [CrossRef]
40. Al-Kheetan, M.J.; Rahman, M.M.; Chamberlain, D.A. Fundamental interaction of hydrophobic materials in concrete with different moisture contents in saline environment. *Constr. Build. Mater.* **2019**, *207*, 122–135. [CrossRef]
41. Almusallam, A.A.; Khan, F.M.; Dulaijan, S.U.; Al-Amoudi, O.S.B. Effectiveness of surface coatings in improving concrete durability. *Cem. Concr. Compos.* **2003**, *25*, 473–481. [CrossRef]
42. Wang, H.; Li, Q. Effect of Pore Water on the Compressive Strength of Wet Concrete. *Eng. Mech.* **2006**, *23*, 141–144.

43. Zhang, G.; Xie, Q.; Chi, J.; Chen, Y.; Zheng, H.; Ma, C.; Zhang, G. Tree root-inspired robust superhydrophobic coatings with high permeation for porous structures. *iScience* **2021**, *24*, 103197. [CrossRef] [PubMed]
44. Jin, H.; Tian, L.; Bing, W.; Zhao, J.; Ren, L. Bioinspired marine antifouling coatings: Status, prospects, and future. *Prog. Mater. Sci.* **2022**, *124*, 100889. [CrossRef]
45. Chen, Y.; Wang, R.; Wang, H.; Hu, F.; Jin, P. Study on PVA-siloxane mixed emulsion coatings for hydrophobic cement mortar. *Prog. Org. Coat.* **2020**, *147*, 105775. [CrossRef]
46. *GB/T 50082-2009*; Standard for Test Methods of Long-Term Performance and Durability of Ordinary Concrete. Standardization Administration of China (SAC): Beijing, China, 2009.
47. *GB 50010-2010*; Code for Design of Concrete Structures. Standardization Administration of China (SAC): Beijing, China, 2009.
48. Garbacz, A.; Górka, M.; Courard, L. Effect of concrete surface treatment on adhesion in repair systems. *Mag. Concr. Res.* **2005**, *57*, 49–60. [CrossRef]
49. Garbacz, A.; Courard, L.; Kostana, K. Characterization of concrete surface roughness and its relation to adhesion in repair systems. *Mater. Charact.* **2006**, *56*, 281–289. [CrossRef]
50. Pan, X.; Shi, Z.; Shi, C.; Ling, T.-C.; Li, N. A review on concrete surface treatment Part I: Types and mechanisms. *Constr. Build. Mater.* **2017**, *132*, 578–590. [CrossRef]
51. Liu, J.; Vipulanandan, C. Tensile bonding strength of epoxy coatings to concrete substrate. *Cem. Concr. Res.* **2005**, *35*, 1412–1419. [CrossRef]
52. Guo, S.-Y.; Luo, H.-H.; Tan, Z.; Chen, J.-Z.; Zhang, L.; Ren, J. Impermeability and interfacial bonding strength of TiO_2-graphene modified epoxy resin coated OPC concrete. *Prog. Org. Coat.* **2021**, *151*, 106029. [CrossRef]
53. *SL 352-2006*; Test Code for Hydraulic Concrete. China Water & Power Press: Beijing, China, 2006.
54. Jalilian, E.; Terryn, H.; Van Assche, G. Water permeation in coatings. *J. Coat. Technol. Res.* **2020**, *17*, 1437–1445. [CrossRef]
55. Wang, Y.; Fan, X.; Wu, R.; Lin, H.; Feng, W. Experimental study on long-term impermeability of recycled aggregate concrete mixed with crystalline admixture and waste glass powder. *J. Clean. Prod.* **2024**, *458*, 142551. [CrossRef]
56. Zheng, Z.; Wang, G.; Yang, C.; Ma, H.; Yin, L.; Liao, Y.; Zhao, K.; Zeng, Z.; Li, H.; Han, Y. A novel nano-grade organosilicon polymer: Improving airtightness of compressed air energy storage in hard rock formations. *Int. J. Min. Sci. Technol.* **2024**, *34*, 305–321. [CrossRef]

Disclaimer/Publisher's Note: The statements, opinions and data contained in all publications are solely those of the individual author(s) and contributor(s) and not of MDPI and/or the editor(s). MDPI and/or the editor(s) disclaim responsibility for any injury to people or property resulting from any ideas, methods, instructions or products referred to in the content.